Challenging the Cloud-Contamination Problem in Flood Monitoring with NOAA/AVHRR Imagery

Yongwei Sheng, Yafang Su, and Qianguang Xiao

Abstract

NOAA/AVHRR (Advanced Very High Resolution Radiometer) data have the potential for flood monitoring due to their high time resolution and low cost. Cloud-free images are quite rare during flood periods. Therefore, cloud contamination is one of the main obstacles to flood monitoring with AVHRR data. Taking into consideration the spectral characteristics of the main ground-cover types during floods, and satellite signal components, this paper discusses a conceptually simple but practically effective method for water identification using AVHRR data. Water bodies can be identified not only in cloud-free areas, but also under semi-transparent clouds and in cloud shadows with this method. This method was applied successfully in the 1991 flood disaster in the Huaihe River Basin in China.

Introduction

Since the potential of NOAA-2/VHRR (Very High Resolution Radiometer, later updated to AVHRR) data for flood monitoring was demonstrated by Wiesnet *et al.* (1974) in mapping the 1973 Mississippi River flood, there have been many noteworthy applications of AVHRR data in this field. Cao *et al.* (1987) analyzed the Liaohe River flood process by interpreting three-channel color-composite images visually. Rasid and Paramanik (1990) employed visual interpretation to monitor 1987 and 1988 Bangladesh floods, using the knowledge of the local environmental setting. Lin (1989) extracted waterlogging information using channel 2. Ali (1989) demonstrated success in mapping the 1984 Bangladesh flood by comparing AVHRR visible, near infrared, and thermal infrared channels. Xiao and Chen (1987) succeeded in identifying flood water using the difference between channel 2 and channel 1, and computed the area of the flood accurately. Barton and Bathols (1989) found that an AVHRR night image of brightness temperature derived from AVHRR channel 4 delineated water bodies quite well in the case of the 1988 Darling River flood. All of the above methods require totally cloud-free AVHRR imagery to monitor flooding. However, cloud contamination during flood periods is usually too severe to allow these methods to work effectively.

Flooding usually results from extraordinary rainfall; thus, it is often cloudy during flooding. Moreover, AVHRR's large ground coverage increases the likelihood of cloud contamination. Consequently, it is rather difficult to find totally cloud-free imagery during flooding. Cloud contamination is one of the main obstacles to flood monitoring using AVHRR. Indeed, Rasid and Paramanik (1990) pointed out that a serious limitation of using AVHRR data or any other satellite optical imagery for monitoring a flood is the lack of availability of cloud-free imagery during floods. If cloud contamination cannot be reduced, the cloud-contaminated image is not useful because water bodies cannot be identified correctly. Thus, dynamic flood processes can not be detected. Although some prior work has dealt with cloud effects in AVHRR data (Kaufman, 1987; Gower 1985), there was no solution to the cloud-contamination problem in AVHRR flood monitoring until Sheng and Xiao (Sheng *et al.* 1993; Sheng and Xiao, 1994a; Sheng and Xiao, 1994b) developed the CH_2/CH_1 scheme in 1993. This paper summarizes this simple but effective method and examines its effectiveness in the case of the 1991 flood disaster in the Huaihe River basin, China.

Y. Sheng is with the Department of Environmental Science, Policy and Management, University of California at Berkeley, Berkeley, CA 94720-3114.

Y. Su is with the Monterey Bay Aquarium Research Institute, Moss Landing, CA 95039-0628 (syf@mbari.org).

Q. Xiao is with the National Satellite Meteorological Center of China, Beijing, China, 100081.

Cloud-Contamination Screening

To evaluate the effect of cloud contamination, cloud-contaminated areas must be identified, including clouds and cloud shadows.

Cloud Screening

There are several algorithms for cloud screening in AVHRR imagery (Coakley and Bretherton, 1982; England and Hunt, 1985; Saunders, 1986; Saunders and Kriebel, 1988). Saunders (1986) concluded that a combination of the spatial coherence method at infrared wavelength and dynamic visible threshold methods, which was referred to as the Spatial Coherence Visible (SVC) approach, proved to be the most effective scheme for day-time use except for uniform thin cirrus. An interactive SVC algorithm was employed in this paper.

Despite the significant difference in spectral reflectance between clouds and the Earth's surface, it is rather difficult to mask clouds from the Earth's surface due to the high variability in cloud expression. Therefore, integrated interpretation should be made based on the visible, infrared, and thermal infrared channels provided by AVHRR. Because the spatial variance of cloud top temperature is greater than that of the Earth's surface, the contextual feature of surface temperature is also used in cloud screening. The contextual feature is here defined as the standard deviation of a 3 by 3 neighborhood in channel 4 (10.5 to 11.5μm): i.e.,

$$F = \sqrt{\frac{1}{9} \sum_{i=1}^{9} (V_i - \overline{V})^2}$$

where V_i, $i=1, 2, \ldots, 9$ is the brightness temperature in the neighborhood, and $\overline{V}$ is the mean.

Photogrammetric Engineering & Remote Sensing, Vol. 64, No. 3, March 1998, pp. 191–198.

0099-1112/98/6403-191$3.00/0

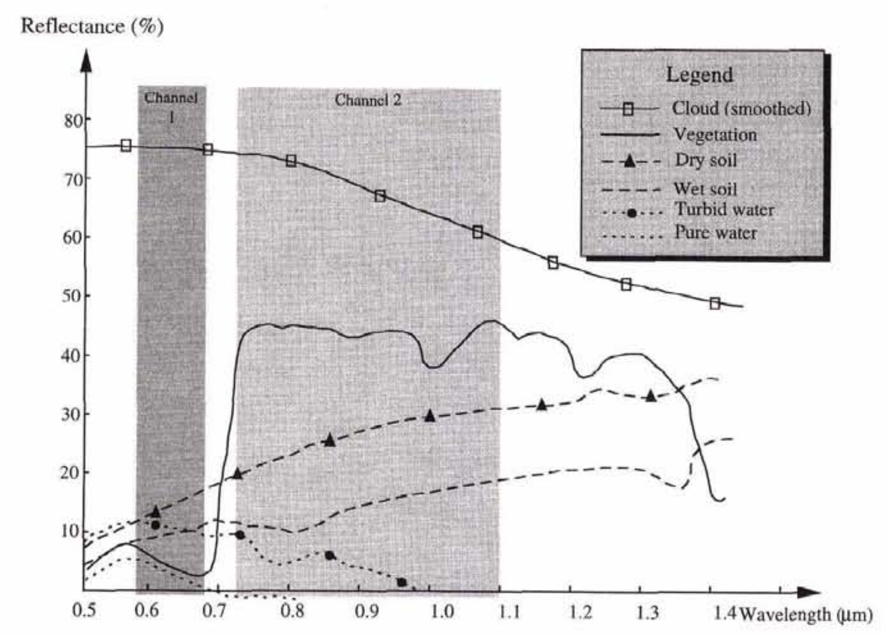

Figure 1. Typical spectral reflectance curves of the main ground-cover types during floods.

Specifically the following aspects are considered in cloud screening:

{*CON1*: $CH_1 > Th_1$}, where CH_1 is albedo in the visible channel;
{*CON2*: $CH_2 > Th_2$}, where CH_2 is albedo in the near infrared channel;
{*CON3*: $CH_4 > Th_3$}, where CH_4 is the brightness temperature in the thermal infrared channel; and
{*CON4*: $F > Th_4$}, where F is the contextual feature in the thermal infrared channel.

Th_1, Th_2, Th_3, and Th_4 are the thresholds which can be selected interactively in order to obtain a satisfactory result. Clouds can consequently be masked as the intersection of the above conditions: i.e.,

$$Cloud = \{CON1\} \cap \{CON2\} \cap \{CON3\} \cap \{CON4\}.$$

Cloud Shadow Identification

Cloud shadows represent another kind of cloud contamination in flood monitoring. Land and water in cloud-shaded areas are difficult to distinguish because there is reduced solar irradiance in cloud-shadowed areas. In addition, the similarity between cloud shadow and water bodies in cloud-free areas in the near-infrared channel makes it difficult to distinguish them.

The procedure to identify cloud shadow is designed based on two aspects: spectral feature and shadow area simulation.

Spectral Feature

Ground cover in cloud shadows receives low irradiance in both the visible and near-infrared channels, which can be considered as a prerequisite in cloud shadow screening.

{*CON1*: $CH_1 < Th_1$}, where CH_1 is albedo in the visible channel;
{*CON2*: $CH_2 < Th_2$}, where CH_2 is albedo in the near infrared channel.

Shadow Area Simulation

Cloud shadow location is a function of cloud location, cloud height, solar angle, and sensor angle. Cloud-shaded area (CSA) can be approximately simulated according to cloud location, solar angle, sensor angle, and assumed cloud height. This aspect can act as another prerequisite for cloud shadow identification:

{*CON3*: *Pixel* $\in$ CSA}.

The cloud shadow can be identified as the intersection based on the above conditions:

$$Shadow = \{CON1\} \cap \{CON2\} \cap \{CON3\}.$$

Water Body Identification

Flooding usually occurs during periods when vegetation is very luxuriant. At the observation scale of NOAA meteorological satellites (1.1-km nominal spatial resolution at nadir), water, vegetation, and soil are the main ground-cover types observed during floods. The recognition of ground-cover types in remotely sensed imagery is based on spectral characteristics. The spectral characteristics of the main ground-cover types are illustrated in Figure 1, as a combination of Swain's ground cover curves (Swain and Davis, 1978) and Davis' cloud reflectance curve (Davis *et al.*, 1984).

During floods, water body albedo increases significantly, with its maximum reflectance peak moving towards the red band because silt and debris concentrate in water; on the other hand, the increased soil moisture decreases soil albedo. Consequently, the reflectance characteristics of ground covers become quite complicated during floods, preventing water and land to be easily distinguished in individual AVHRR channels. Water shows low albedo in the near infrared band (AVHRR channel 2), while vegetation and other objects in land have high albedoes. In contrast to channel 2, vegetation in the red band (AVHRR channel 1) has relatively low albedo compared with soil and turbid water, while wet soil and water have similar reflectance characteristics in the red band. Therefore, the ratio band of channel 2 to channel 1 can be used to enhance the difference between water (pure and turbid) and land (vegetation and soil), and to distinguish them effectively.

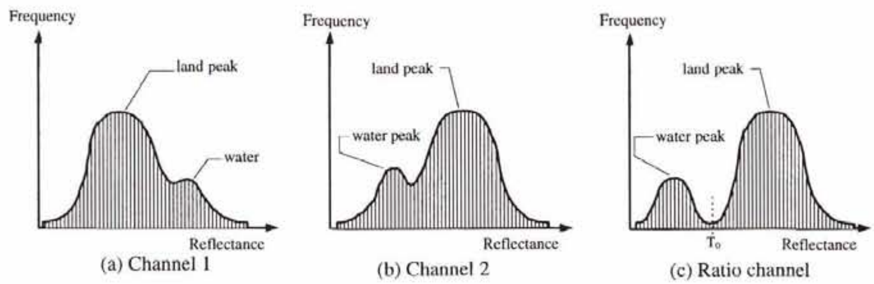

Figure 2. AVHRR typical histograms in flooded areas.

Hence,

$$R = k * \frac{CH_2}{CH_1},$$

where k is the amplified coefficient, which is assigned to 128 in this study.

The typical histograms of channel 1, channel 2, and ratio channel during floods are shown in Figure 2. Water and land are not easy to separate in individual channels because the difference between them is not great enough, as illustrated in their histograms (Figures 6a and 6b). A noteworthy bimodal distribution can be found in the histogram of the ratio channel, in which water has a low value (water peak) and land has an extremely high value (land peak). The two peaks can be easily separated by a threshold T_0. The threshold value T_0, which is located between the two peaks in the histogram, can be determined interactively to identify water bodies as follows:

$$\begin{cases} Water, & \text{if } R \le T_0 \\ Land, & \text{otherwise} \end{cases}$$

It is encouraging that the ratio band of CH_2/CH_1 can identify water bodies not only in cloud-free area but also under thin cloud cover and in cloud shadow.

Cloud Influence Elimination

Over 50 percent of the Earth's surface is typically covered by clouds at any time (Paltridge and Platt, 1976). In many temperate regions, persistent cloud cover may limit cloud-free large-area coverage to only a few scenes per year (Tabata and Gower, 1980). During floods, the situation becomes even worse, and cloud-free images are rare. The cloud influence is one of the main obstructions to flood monitoring using AVHRR data. AVHRR cannot sense the Earth's surface under thick cloud cover. No method can be expected to eliminate cloud contamination to obtain flood information in this situation. In the case of thin cloud cover, the sensor does receive some information from the underlying surface, mixed with cloud information. Moreover, spectral characteristics of water and land are so different that it is possible to distinguish water from land under thin cloud cover even though contamination still exists. When cloud contamination is not very severe (thin clouds), some of the cloud influence (including cloud and cloud shadows) can be removed in the ratio band of CH_2/CH_1.

Water Identification Under Cloud

In the area covered by a semi-transparent cloud (thin cloud), as Figure 3 shows, the reflective value obtained by the satellite sensor contains information from both the cloud and the ground underneath, besides path radiance (scattered by substance other than cloud): that is;

$$CH_i = C_i + G_i + P_i$$

where

i is the channel number, i=1, 2;
CH_i is the value obtained by satellite sensor in channel i;
C_i is the contribution from clouds;
G_i is the contribution from the ground; and
P_i is atmospheric path radiation, which is very close to zero in the near-infrared channel.

Therefore, the ratio of CH_2/CH_1 is given by

$$R = k * \frac{CH_2}{CH_1} = k * \frac{C_2 + G_2 + P_2}{C_1 + G_1 + P_1}.$$

For water,

$$R(Water) = k * \frac{C_2 + G_2\,(Water) + P_2}{C_1 + G_1\,(Water) + P_1}$$

while, for land,

$$R(Land) = k * \frac{C_2 + G_2\,(Land) + P_2}{C_1 + G_1\,(Land) + P_1}.$$

According to the spectral characteristics of land and water (Figure 1), $G_1(Water)$ is usually greater than $G_1(Land)$, while $G_2(Water)$ is commonly less than $G_2(Land)$. Thus, $R(Water) < R(Land)$. This critical result demonstrates that water and land underneath thin clouds have different values in

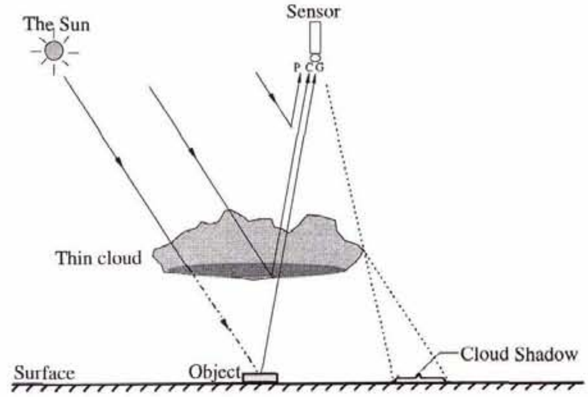

Figure 3. Diagram of satellite signal components in the case of thin cloud cover.

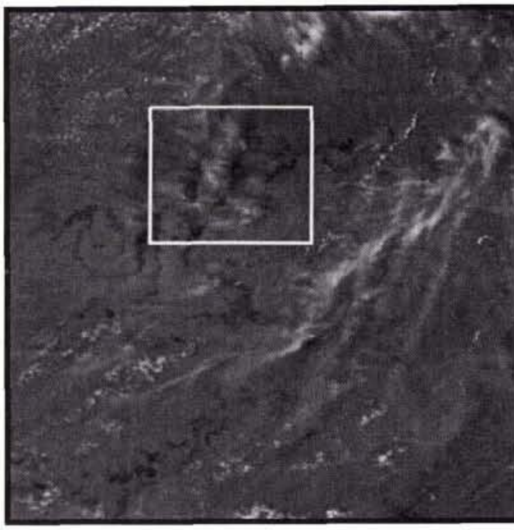

Figure 4. Channel 2 of NOAA-11, 18 July 1991.

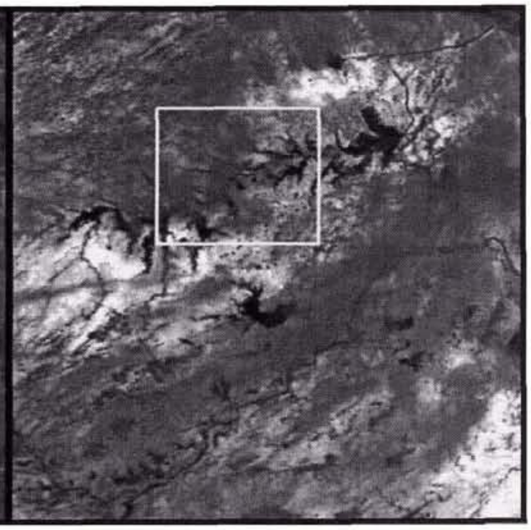

Figure 5. The ratio band of CH_2/CH_1.

the ratio band. Therefore, it is possible to distinguish water from land with the ratio band in the case of thin cloud cover.

Water Identification in Cloud Shadow

In the cloud-shaded area, the ground cover receives scattered sunlight, but illumination is not sufficient to show much difference among ground covers. It is hardly possible to separate water and cloud-shaded land in channel 2, which is commonly used to delineate water bodies.

$$CH_i = G_i + P_i$$

where

i is the channel number, $i=1$, 2;

G_i is contribution related to scattered irradiance in channel i; and

P_i is contribution of path radiance in channel i.

Therefore, the ratio band is given by

$$R = k * \frac{CH_2}{CH_1} = k * \frac{G_2 + P_2}{G_1 + P_1}.$$

For water,

$$R(Water) = k * \frac{G_2(Water) + P_2}{G_1(Water) + P_1}$$

while, for land,

$$R(Land) = k * \frac{G_2(Land) + P_2}{G_1(Land) + P_1}.$$

In cloud shadow, the sensor records a slightly higher value for water than for land in channel 1 ($G_1(Water) > G_1(Land)$), though the difference is not sufficient to distinguish them. Furthermore, $G_2(Water)$ is less than $G_2(Land)$. Thus, $R(Water)$ is much less than $R(Land)$. The difference between water and land in the ratio image might be large enough to separate them in cloud shadow.

Threshold Selection

The choice of threshold T_0 is very critical in order to separate water and land in the ratio band. Though T_0 can be determined interactively on a computer, the possible range of T_0 may be estimated theoretically.

In Cloud-Free Areas

In cloud-free areas, $R(Land) >> R(Water)$ ($R(Land)$ is much larger than $R(Water)$) and $G_2(Water) << G_1(Water)$ result in $R(Water) << k$ for water, and similarly a result of $R(Land) >> k$ can be reached for land. Therefore, a T_0 close to k is expected to separate water and land. In this case, $R(Water)$ and $R(Land)$ are usually so different that T_0 has a flexible range and is easy to determine.

Under Cloud Cover

As shown in Figure 1, cloud reflectivity is similar in AVHRR channels 1 and 2; that is, $C_1 \approx C_2$. In the case of a thick cloud, both C_1 and C_2 are very large, and the ground contribution is close to zero. Therefore,

$$R(Water) = R(Land) = k * \frac{C_2 + P_2}{C_1 + P_1} \approx k * \frac{C_2}{C_1},$$

which means that no threshold can separate water and land.

For a thin cloud situation when C_1 and C_2 are not very large, $G_1(Water)$ and $G_2(Water)$, $G_1(Land)$ and $G_2(Land)$ can affect $R(Water)$ and $R(Land)$, respectively. $G_1(Water) > G_2(Water)$ and $P_2 \rightarrow 0$ produce $R(Water) < k$. Similarly, $G_2(Land) > G_1(Land)$ leads to $G_2(Land) + P_2 \geq G_1(Land) + P_1$ and $R(Land) \geq k$. Therefore, T_0 should be slightly less than k or approximately equal to k.

In Cloud Shadow

The ratio value mainly depends on G_1 and G_2. Because $G_1(Water) > G_2(Water)$ and $P_2 \rightarrow 0$, $R(Water) < k$. For land, $G_2(Land) > G_1(Land)$ leads to $G_2(Land) + P_2 \geq G_1(Land) + P_1$ and $R(Land) \geq k$. Therefore, T_0 should be slightly less than k or approximately equal to k.

Theoretically, a value of T_0 which is slightly less than k or approximately equal to k can help to identify water bodies for all the above three situations.

Results and Discussion

From the late spring to the early summer of 1991, the Yangtze and Huaihe river basins of China were hit by torrential rainstorms, with precipitation totaling 700 to 1200mm (2 to 3 times greater than normal). The recorded water levels at many hydrologic stations in the above regions approached the highest levels in history, and the rise of the water level

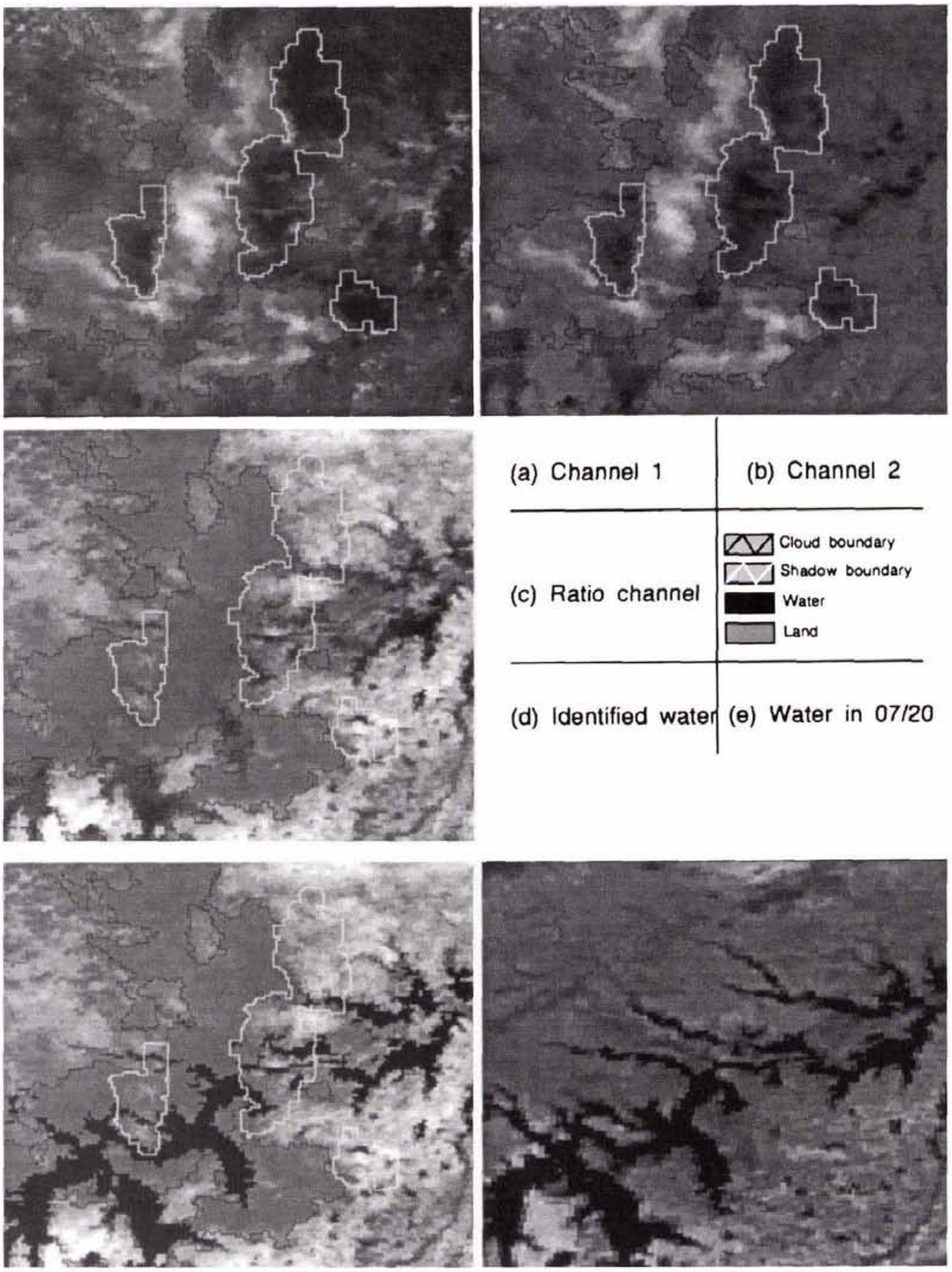

Figure 6. Cloud contamination elimination analysis in window.

in rivers, lakes, and reservoirs caused the most severe flood disaster in a century. There were scarcely any totally cloud-free images for nearly two months during this inundation. In the seriously damaged regions, only seven usable AVHRR images were found, due to the severe and widespread cloud contamination in the other images, even though NOAA satellites passed over twice daily. Among these seven images, five were still contaminated by clouds to a varying degree. There were some regions locally covered by thin clouds in the NOAA-11 image on 18 July (see channel 2 in Figure 4), which provides a good case study. In the ratio image (Figure 5), some of the cloud contamination has been eliminated, and the rivers and other water bodies are revealed under clouds in the ratio band.

Subwindow Analysis

To validate the effect of water identification and cloud influence elimination, a 140- by 160-pixel subwindow (lower-left corner (116.40°E, 32.25°N) to upper-right corner (118.00°E, 33.65°N)) in the seriously damaged region (squared by the white line in Figure 5) with clouds and shadow was selected for detailed study.

Channel 1, channel 2, and the ratio band of CH_2/CH_1 in the window are shown in Figures 6a, 6b, and 6c, respec-

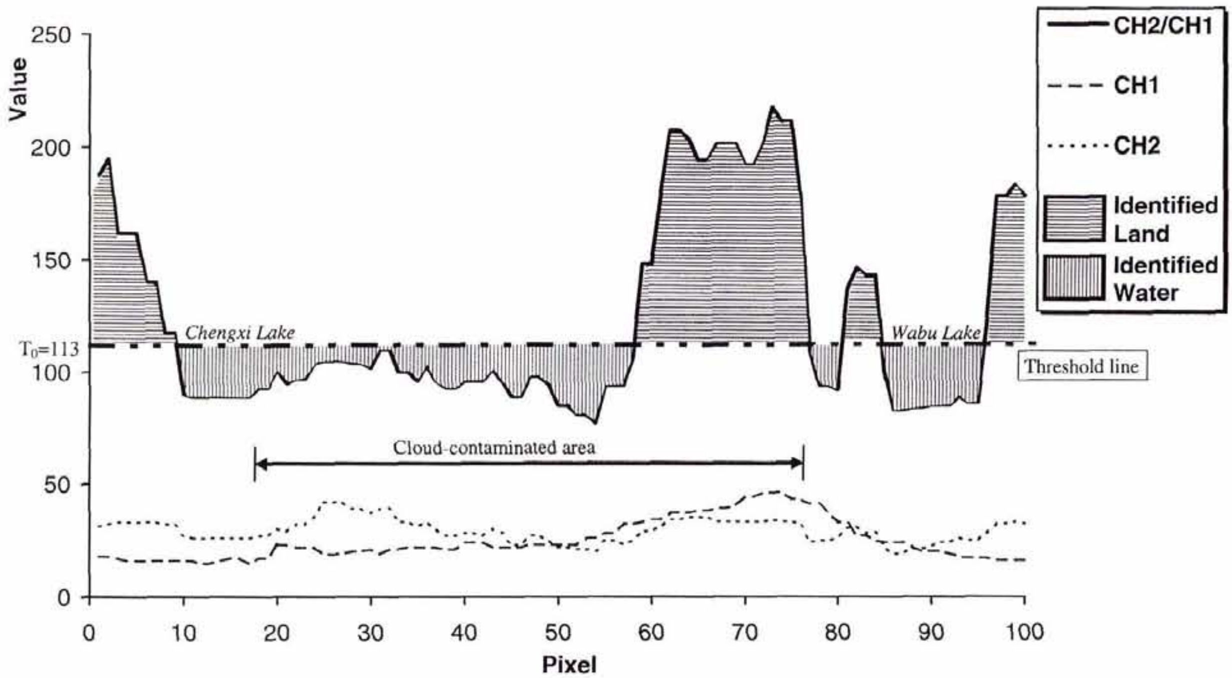

Figure 7. Profile analysis for cloud contamination elimination.

tively, where the areas surrounded by black lines are clouds and the areas circled by white lines are cloud shadows. It is evident that the water-body boundaries in the cloud-free region are not very clear. Clouds have high values in both channel 1 and channel 2, while the cloud-shadow area has an extremely low value. It is impossible to identify water bodies under clouds or in cloud shadow with either channel 1 or channel 2. Therefore, the individual channel is ineffective in distinguishing water bodies from land. In the ratio band of CH_2/CH_1, the water boundary in the cloud-free region is very clear, and some cloud contamination is eliminated. Water information can be extracted under clouds and in cloud shadow when the cloud is not very thick. With an appropriate threshold (T_0=113 here), most water bodies under clouds or in cloud shadow and in cloud-free areas can be identified effectively. The result is shown in Figure 6d, where the black color represents the identified water bodies. Water-body boundaries between cloud-contaminated areas and cloud-free areas are connected smoothly. The identified water bodies correspond well to the result (Figure 6e) from cloud-free AVHRR imagery of two days later (20 July) when there was no remarkable rainfall in the previous two days. This consistency shows the success of this method in water-body identification under cloud-contamination situations.

Profile Analysis

Profile analysis was carried out along a transect from Zhouji (115.98°E, 32.45°N) to Caoan (116.98°E, 32.45°N) in Figure 7. This profile line passes through the Chengxi flood-storage area, cropland, and Wabu Lake. The cloud contamination in the middle area results in irregular sharp variation in all three profiles (CH_2, CH_1 and ratio band). From the profiles of channel 1 and channel 2, one can see that it is impossible for an individual channel to distinguish water and land due to cloud contamination, no matter what threshold is selected. Significant difference between water and land is shown in the profile of the ratio band, and the cloud contamination is depressed. Water (below the threshold line) and land (above the threshold line) are satisfyingly separated with the appropriate threshold T_0 of 113. Comparing these three profiles, one can find that the ratio profile slope is much sharper around the water/land boundary than those of the CH_2 and CH_1 profiles. The threshold for CH_2 or CH_1 is too sensitive to locate boundaries effectively. The variation of threshold in the ratio band does not produce much boundary change so that a flexible threshold can be easily determined for the purpose of water-body identification.

Pixel Analysis

Several water and land pixels were randomly sampled to analyze the effectiveness of water identification.

In Cloud-Free Areas

Four water pixels and four land pixels in cloud-free areas were randomly selected as the analyzing samples (Table 1). The inner-group variations of water and land are 9.9 and 27.8 in the ratio band, respectively, while the inter-group distance is 142.25. This shows that the differences of water and land is enhanced. The threshold is easy to determine. Here, as long as $T_0 \in [84, 179]$, water and land can be distinguished correctly.

Thin Cloud Contamination

Table 2 shows the result of pixel analysis under thin clouds. Although the enhanced difference between water and land is not as distinct as that under the cloud-free situation, water bodies, which cannot be identified by an individual channel, become distinguishable in the ratio band with a threshold $T_0 \in [103, 118]$.

In Cloud Shadow

Table 3 shows that reflectance values of water and land in cloud shadow are so similar in individual channels that it is very difficult for channel 1 or channel 2 to separate them.

TABLE 1. ANALYSIS TABLE OF WATER IDENTIFICATION IN CLOUD-FREE AREAS*

Ground cover	land	land	land	land	water	water	water	water
Location	(115.64°,32.79°)	(115.87°,32.19°)	(117.51°,32.26°)	(117.68°,33.46°)	(118.71°,32.29°)	(117.78°,32.99°)	(116.91°,32.35°)	(115.81°,32.55°)
Channel 1	16	14	19	14	51	37	34	32
Channel 2	24	31	31	24	34	18	16	17
Ratio band	180	255	198	204	83	60	58	65
Identified as	land	land	land	land	water	water	water	water

*The identified results in all the Tables are from $T_0 = 113$.

TABLE 2. ANALYSIS TABLE OF WATER IDENTIFICATION IN THIN CLOUD-COVERED AREAS

Ground cover	land	land	land	land	water	water	water	water
Location	(117.31°,32.46°)	(116.44°,32.62°)	(116.68°,32.82°)	(116.91°,33.66°)	(117.21°,32.59°)	(116.83°,32.54°)	(117.11°,32.70°)	(116.61°,32.60°)
Channel 1	36	44	36	40	41	35	31	29
Channel 2	41	42	37	43	32	28	25	24
Ratio band	141	119	128	134	97	99	100	102
Identified as	land	land	land	land	water	water	water	water

TABLE 3. ANALYSIS TABLE OF WATER IDENTIFICATION IN CLOUD SHADOW

Ground cover	land	land	water	water
Location	(117.44°, 33.88°)	(117.61°, 32.59°)	(117.30°, 33.04°)	(117.36°, 33.00°)
Channel 1	11	9	15	14
Channel 2	15	14	9	11
Ratio band	160	179	72	93
Identified as	land	land	water	water

TABLE 4. ANALYSIS TABLE OF WATER IDENTIFICATION IN THICK CLOUD-COVERED AREAS

Ground cover	land	land	water	water
Location	(117.05°, 32.87°)	(117.26°, 33.36°)	(117.01°, 32.97°)	(117.11°, 32.84°)
Channel 1	56	48	56	58
Channel 2	52	49	52	52
Ratio band	116	128	116	112
Identified as	land	land	X land	water

Nevertheless, the difference between water and land is enlarged in the ratio band so significantly that they are readily distinguished.

Thick Cloud Contamination

In the case of thick clouds, there is very little information from the Earth's surface. Even the ratio band method cannot identify water bodies correctly. Table 4 illustrates a misidentification of a water pixel. No optical sensor is expected to handle this situation. The only possible solution is to apply radar technology with cloud-penetrating capabilities as Imhoff did (Imhoff *et al.*, 1987).

Conclusions

NOAA/AVHRR has great potential in large-area flood monitoring due to its high temporal resolution. However, AVHRR is unable to penetrate clouds because it is an optical sensor. The widespread persistent cloud cover during floods seriously limits AVHRR data utility. Cloud contamination is one of the main obstacles to AVHRR flood monitoring. Reducing cloud contamination and identifying water bodies in cloud-contaminated imagery is necessary for effective flood monitoring with AVHRR data.

Though individual AVHRR channels are always affected by the cloud-contamination problem, the ratio band of CH_2/CH_1 is relatively immune to cloud influence. This ratio scheme not only can enhance the difference between water and land, but it also eliminates some of the cloud influence and separates water bodies and land both under thin cloud cover and in shadow. This simple but effective method can help to make full use of AVHRR images during flood periods. Therefore, it is very suitable for flood monitoring. It is necessary to point out that this method is only able to deal with thin cloud cover, and cannot work with thick clouds. Under this condition, cloud-penetrating radar technology is a possible solution. However, it would be necessary to accept the high cost or suffer the low temporal resolution for radar data.

Acknowledgments

The authors would like to thank Michael Westphal and Tom O'Reilly for their contributions in improving the writing style.

References

Ali, A., 1989. Study of river flood hydrology in Bangladesh with AVHRR data, *International Journal of Remote Sensing*, 10(12): 1873–1892.

Barton, I.J., and J.M. Bathols, 1989. Monitoring floods with AVHRR, *Remote Sensing of Environment*, 30(1):89–94.

Cao, S., W. Dong, and Q. Xiao, 1987. Applying meteorological satellite imagery to monitor Liaohe River flood, *Remote Sensing Information*, 1987(3):12–16 (in Chinese).

Coakley, J.A., and F.P. Bretherton, 1982. Cloud cover from high resolution scanner data: detecting and allowing for partially filled fields of view, *Journal of Geophysical Research*, 87(C7):4917–4932.

Davis, P.A., E.R. Major, and H. Jacobowitz, 1984. An assessment of NIMBUS-7 ERB shortwave scanner data by correlative analysis with narrowband CZCS data, *Journal of Geophysical Research*, 89(D4):5077–5088.

England, C.F., and G.E. Hunt, 1985. A bispectral method for the automatic determination of parameters for use in imaging satellite cloud retrievals, *International Journal of Remote Sensing*, 6(9): 1545–1553.

Gower, J.F.R., 1985. Reduction of the effect of cloud on satellite thermal imagery, *International Journal of Remote Sensing*, 6(8): 1419–1434.

Imhoff, M.L., C. Vermillion, M.H. Story, A.M. Choudhury, A. Gafoor, and F. Polcyn, 1987. Monsoon flood boundary delineation and damage assessment using space borne imaging radar and Landsat data, *Photogrammetric Engineering & Remote Sensing*, 53(4): 405–413.

Kaufman, Y., 1987. The effect of subpixel clouds on remote sensing, *International Journal of Remote Sensing*, 8(6):839–857.

Lin, C., 1989. Applying meteorological satellite information to monitor waterlogging in Heilongjiang Province, *Remote Sensing Information*, 1989(3):24–28 (in Chinese).

Paltridge, G.W., and C.M.R. Platt, 1976. *Radioactive Processes in Meteorology and Climatology*, Elsevier, New York, pp. 32–34.

Rasid, H., and M.A.H. Paramanik, 1990. Visual interpretation of satellite imagery for monitoring floods in Bangladesh, *Environmental Management*, 14(6):815–821.

Saunders, R.W., 1986. An automated scheme for the removal of cloud contamination from AVHRR radiances over western Europe, *International Journal of Remote Sensing*, 7(7):867–886.

Saunders, R.W., and K.T. Kriebel, 1988. An improved method for detecting clear sky and cloudy radiances from AVHRR data, *International Journal of Remote Sensing*, 9(1):123–150.

Sheng, Y., Q. Xiao, and W. Chen, 1993. Method on flood monitoring using AVHRR data, *Proceedings of the 6th European AVHRR Users Meeting*, Belgirate, Italy, pp. 293–302.

Sheng, Y., and Q. Xiao, 1994a. Water identification in cloud-contaminated NOAA/AVHRR imagery, *Remote Sensing of Environment in China*, 9(4):247–255 (in Chinese).

———, 1994b. Progress on flood monitoring using meteorological satellites in china, *Satellite Applications*, 2(2):36–40 (in Chinese).

Swain, P.H., and S.M. Davis, 1978. *Remote Sensing: The Quantitative Approach*, McGraw-Hill Inc., New York, pp. 227–289.

Tabata, S., and J.F.R. Gower, 1980. A comparison of ship and satellite measurements of sea surface temperature off the Pacific coast of Canada, *Journal of Geophysical Research*, 85(C11):6636–6648.

Wiesnet, D.R., D.F. McGinnis, and J.A. Pritchard, 1974. Mapping of the 1973 Mississippi River floods by NOAA-2 satellite, *Water Resources Bulletin*, 10(5):1040–1049.

Xiao, Q., and W. Chen, 1987. Songhua River flood monitoring with meteorological satellite imagery, *Remote Sensing Information*, 1987(4):37–41 (in Chinese).

(Received 10 October 1996; revised and accepted 17 June 1997; revised 20 August 1997)